International Forum on Aeroelasticity and Structural Dynamics
IFASD 2017
25-28 June 2017 Como, Italy

DYNAMIC GAIN SCHEDULING OF HIGHLY FLEXIBLE AIRCRAFT APPLYING ADAPTIVE CONTROL

Rafael M. Bertolin[1], Flávio J. Silvestre[1], Antônio B. Guimarães Neto[1], Guilherme C. Barbosa[1], Pedro J. González R.[1], Carlos E. S. Cesnik[2]

[1]Department of Aerospace Engineering
Instituto Tecnológico de Aeronáutica
São José dos Campos, SP, 12228-900, Brazil
rafaelmb@ita.br
flaviojs@ita.br
antoniobgn@gmail.com
guichavesbarbosa@gmail.com
pedrojgonzalezr@gmail.com

[2]Professor of Aerospace Engineering, Department of Aerospace Engineering
University of Michigan
Ann Arbor, Michigan 48109-2140, USA
cesnik@umich.edu

Keywords: adaptive control, model reference adaptive control, Lyapunov direct method, control of flexible aircraft, hale aircraft

Abstract: In this paper, the application of adaptive control is demonstrated for highly flexible aircraft in a dynamic gain scheduling approach. For that, an adaptive control law is designed for the stability augmentation system, taking as reference model the closed-loop dynamics provided by a baseline controller. Global stability is demonstrated by the Lyapunov direct method. Closed-loop nonlinear simulations are performed. The performance of the control system is evaluated considering the aircraft in high loading operations, specifically in accelerated turning maneuvers. Overall, this control strategy proved to overcome instabilities arising when linear control is applied, while conferring the aircraft adequate time response.

1 INTRODUCTION

The interest in the class of unmanned vehicle known as High-Altitude and Long-Endurance (HALE) aircraft has been growing in the lastest years. The mission profile of a HALE aircraft involves cruising at very high altitudes, and very-long endurance flights (during days, weeks and even months), whether for military or civilian applications [1, 2]. The most recent example of application of a HALE aircraft is Aquila, a solar-powered airplane designed by the Facebook Connectivity Lab to be used to bring affordable internet in hardest-to-reach places. When complete, Aquila will be able to circle a region up to 60 miles in diameter, beaming connectivity down from an altitude of more than 60.000 feet and flying for up to three months at a time [3].

The problem is that, due the mission requirements, the HALE aircraft have become so lightweight and flexible that the vehicle may invariably undergo large deformations during operation, exhibiting a nonlinear behaviour, not only due to Euler angles and gravity force decomposition,

but more importantly due to structural and aerodynamic responses. For this reason, nonlinear aerodynamic and structural modelling is necessary, and linear control design techniques are no longer adequate [4]. In recent years, several techniques to modeling dynamics of very flexible aircraft have been proposed [5–7]. At the same time, differente testbeds have been built in order to validate such models [8]. The most recente of them is the University of Michigan X-HALE, which is currently being operated at ITA in Brazil.

Very flexible aircraft are caracterized by very low frequencies of their natural structural vibration modes and, as a result, a strong and dangerous coupling between the structural dynamics and the rigid-body flight dynamics occurs, giving rise to a series of challenges for flight control law design.

Adaptive control seems to be an appropriate approach for highly flexible aircraft, since with large deformations the plant to be controlled varies significantly. Those variations can occur due to several factors such as actuator anomalies during long-endurance flights, dihedral angle changes, model uncertainties and gust wind inflows, and adaptive control should be able to overcome this adversities.

The interest in adaptive control emerged in the aerospace industry in the early 1950s motivated by the design of autopilots for aircraft that operated in a wide flight envelope, with large range of speeds and altitudes. Different flight conditions cause the aircraft dynamics to change significantly [9]. A notorious case-study was reported by Dydek et al. [10], where the hypersonic vehicle X-15-3 designed by NASA makes use of an adaptive control law. The X-15-3 was one of the first aircraft to present an adaptive controller, but a fatal accident occurred on November 15th, 1967. The experiment revealed that a satisfactory adaptive control law can be designed without having accurate information about the aircraft parameters and without an analytical proof of stability, although the necessity of the latter was reinforced by the fatal accident. In the same paper, a new approach is proposed, in which the asymptotic stability is ensured. The new results showed that the resulting controller would be able to reach performance and stability, even in the presence of similar failures that led to the accident of X-15-3.

Ponnusamy and Guibe [11] proposed an adaptive output feedback control design based on a flexible aircraft model considering a simply rigid reference model. The presented results are promising and attested the efficiency of setting up a simple reference model, even for highly complex models.

To deal with uncertainties in the model, Qu, Lavretsky, and Annaswamy [12] design an adaptive controller to be added to a baseline linear one, developed for a very flexible aircraft flying under nominal conditions. Global stability and asymptotic tracking of the overall adaptive controller designed was ensured and validated using nonlinear simulations.

In this paper, the advantages of adaptive control for very flexible aircraft will be demonstrated for the X-HALE aircraft in a dynamic gain scheduling approach. For that, the aircraft will be considered in high loading operations, specifically in accelerated turning maneuvers. The adaptive law will be designed based on the Lyapunov stability theorems. Nonlinear simulations in closed-loop demonstrated that while linear control fails in assuring stability for the velocity range of interest, the adaptive controller stabilises the plant without loosing performance.

2 THEORICAL DEVELOPMENT

2.1 Problem description

If the true parameters of a real plant are substantially different from the assumed ones in the control law design process, system instabilities may occur. An example is presented in Fig. 1, where a stability augmentation system (SAS) coupled with a robust linear controller designed for velocity, altitude, sideslip and roll angle tracking of a highly flexible aircraft fails for a variation of $4m/s$, probably due to nonlinearities present in the plant [13].

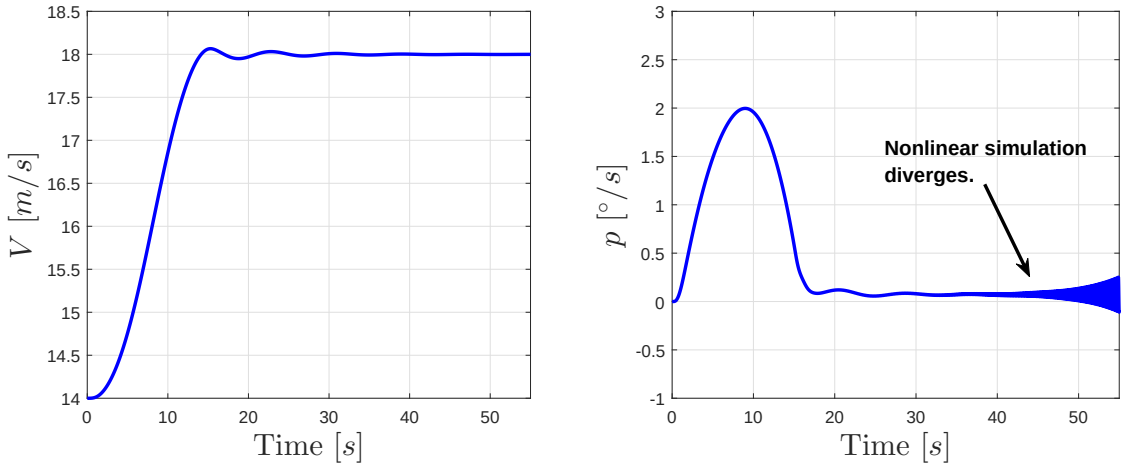

Figure 1: Divergence of the control system for velocity tracking of a very flexible aircraft.

Particularly in the aforementioned example, the stability augmentation inner-loop designed for the operating point of $14m/s$ becomes unstable when the vehicle approached the flight condition of $18m/s$. Even when the system remains stable, its closed-loop tracking performance may deteriorate to a point of becoming unacceptable.

It is known that a wide range of linear control techniques can be employed to address this issue, such as robust control, that explicitly deals with system's uncertainty, or gain schedule which is a strategy for controlling systems whose dynamics change with time or operating condition [14].

The problem with the linear approach is that it is only valid for small disturbances around an equilibrium point. In the case of highly flexible aircraft, however, this small disturbances can be sufficiently large to change significantly the plant and, therefore, the assumption of linearity may no longer be valid.

Consider the classical tracking problem as illustred in Fig. 2 [14]. The closed-loop plant control signal is:

$$\mathbf{u} = \mathbf{u_c} - \mathbf{u_{sas}} \tag{1}$$

where $\mathbf{u_c}$ corresponds to the compensator output control signal, designed to keep small the compensator input tracking error signal ($\mathbf{e_y}$), which in turn is defined by a unity-gain outer loop that feeds the performance output ($\mathbf{y_{trck}}$) back and subtracts it from the reference command ($\mathbf{y_{cmd}}$). The performance output is defined by the tracking output selection matrix $\mathbf{C_{trck}}$.

The inner-loop corresponds to the SAS signal $\mathbf{u_{sas}}$, defined as:

$$\mathbf{u_{sas}} = \mathbf{K^T y_{sas}} = \mathbf{K^T C_{sas} y} \tag{2}$$

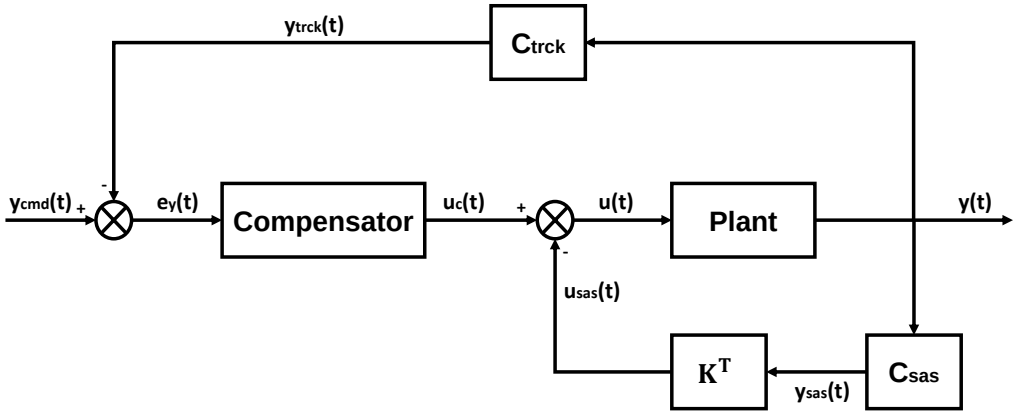

Figure 2: Block diagram of the classical tracking problem. Adapted from [14].

designed to regulate the output of the system to an equilibrium point, ensuring closed-loop stability and desirable time-response characteristics. $\mathbf{C_{sas}}$ corresponds to the SAS measurement selection matrix.

The main idea behind the model reference adaptive control (MRAC) consists in designing a controller whose SAS gains $\mathbf{K^T}$ are updated online using adaptive law. The adjustments of the gains is accomplished in real-time based on the difference between the ideal response of a closed-loop reference model and the real response of the plant. Both responses are due to external commands $\mathbf{y_{cmd}}$, giving rise to a state tracking error (e) which subsequently is sent to the adaptive law. Finally, the controller computes the estimated SAS gains $\hat{\mathbf{K}}^{\mathbf{T}}$ based on the system output, state tracking error and design parameters. A block diagram of the MRAC is presented in the Fig. 3.

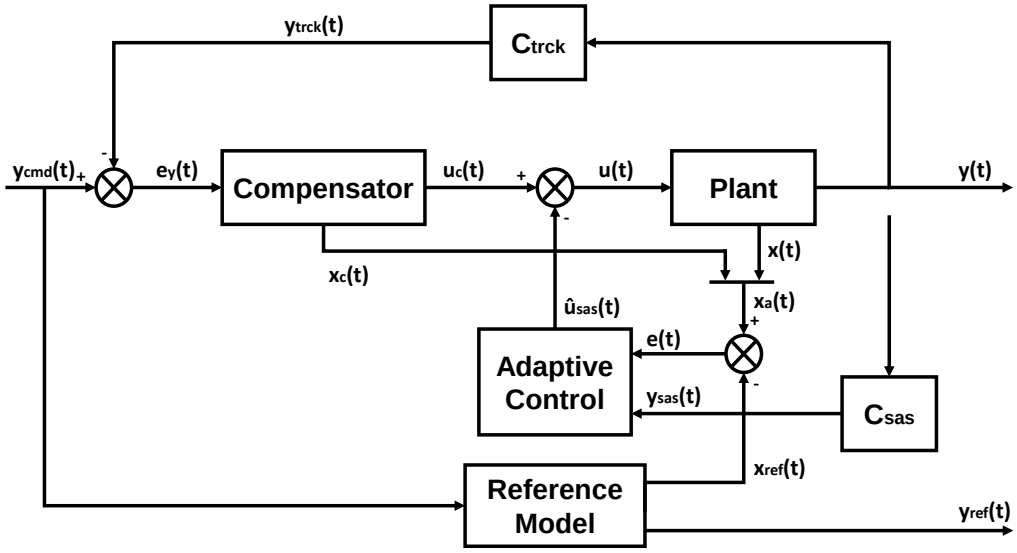

Figure 3: Block diagram of the MRAC applied in a tracking problem.

In the figure above:

$$\hat{\mathbf{u}}_{\mathbf{sas}} = \hat{\mathbf{K}}^{\mathbf{T}}\mathbf{y}_{\mathbf{sas}} = \hat{\mathbf{K}}^{\mathbf{T}}\mathbf{C}_{\mathbf{sas}}\mathbf{y} \tag{3}$$

and the closed-loop control signal, in turn, is:

$$\mathbf{u} = \mathbf{u_c} - \hat{\mathbf{u}}_{\mathbf{sas}} \tag{4}$$

The reference model can be, for example, a baseline closed-loop model of the plant, for a specific flight condition where the control law has been calculated, exhibiting desirable time-response characteristics.

In this way, the adaptive controller acts on the inner-loop and force the system output $\mathbf{y_{trck}}$ to track any bounded time-varying command signal $\mathbf{y_{cmd}}$ keeping the performance of the real closed-loop response similar to the reference model, while operating in the presence of uncertainties and unknown variations of plant parameters. All this is accomplished ensuring bounded state tracking error.

Some aspects to be noted are: first, in the approach here proposed, it is assumed that full state measurement is available; second, the adaptive control acts on the inner-loop but has no direct effect on the outer-loop. Once the latter usually is designed using linear control theory (as will be the case in this work) the complete closed-loop system will still depend on the hypothesis of small perturbations to comply with the principles of linearity. Even if the design of the outer-loop lays on linear control theory, thus assuming small elastic deformations, the adaptive control approach proposed may use a slightly flexible aircraft model as the reference model. Since the inner-loop will act to adjust the aircraft behaviour to that of the reference model, a highly flexible aircraft is expected at some extent to behave as a slightly flexible aircraft.

2.2 MRAC design

Consider a class of multi-input multi-output (MIMO) uncertain systems with the following form:

$$\dot{\mathbf{x}} = \mathbf{A}\mathbf{x} + \mathbf{B}\mathbf{\Lambda}\mathbf{u} \tag{5}$$

$$\mathbf{y} = \mathbf{C}\mathbf{x} \tag{6}$$

where $\mathbf{x} \in \mathbb{R}^{n\times 1}$ is the system state vector, $\mathbf{u} \in \mathbb{R}^{m\times 1}$ is the control input, $\mathbf{y} \in \mathbb{R}^{p\times 1}$ is the system output vector, $\mathbf{A} \in \mathbb{R}^{n\times n}$ is the state matrix, constant and unknown, $\mathbf{B} \in \mathbb{R}^{n\times m}$ is the input matrix, constant and known, $\mathbf{\Lambda} \in \mathbb{R}^{m\times m}$ is a constant diagonal unknown matrix with strictly positive diagonal elements and $\mathbf{C} \in \mathbb{R}^{p\times n}$ is the output matrix known and constant.

The uncertainty in $\mathbf{\Lambda}$ is introduced to model possible control failures or modeling errors, in the sense that there may exist uncertain control gains or the designer may have incorrectly estimated the system control effectiveness [9].

First, it is defined an ideal control solution, as if the unknown parameters aforementioned ($\mathbf{A}$ and $\mathbf{\Lambda}$) were known. For this, suppose a traditional linear control structure similar to the presented in Fig. 2, where the SAS gains $\mathbf{K^T}$ as well as the compensator model were designed using some linear control technique, so that the ideal closed-loop system presents desired stability and performance characteristics. Assuming the following controller model:

$$\dot{\mathbf{x}}_\mathbf{c} = \mathbf{F}\mathbf{x}_\mathbf{c} + \mathbf{G}\mathbf{e}_\mathbf{y} \tag{7}$$

$$\mathbf{u}_\mathbf{c} = \mathbf{H}\mathbf{x}_\mathbf{c} + \mathbf{J}\mathbf{e}_\mathbf{y} \tag{8}$$

where $\mathbf{x_c} \in \mathbb{R}^{n_c\times 1}$ is the compensator state and $\mathbf{F} \in \mathbb{R}^{n_c\times n_c}$, $\mathbf{G} \in \mathbb{R}^{n_c\times p_{trck}}$, $\mathbf{H} \in \mathbb{R}^{m\times n_c}$ and $\mathbf{J} \in \mathbb{R}^{m\times p_{trck}}$ are its state-space realization, it is easy to verify from Equations (1), (2) and (5-8)

that the closed-loop system is given by:

$$\dot{\mathbf{x}} = \underbrace{\left(\mathbf{A} - \mathbf{B\Lambda J C_{trck} C}\right)}_{\mathbf{A_{fw}}} \mathbf{x} - \mathbf{B\Lambda K^T C_{sas} C x} + \mathbf{B\Lambda H x_c} + \mathbf{B\Lambda J y_{cmd}}, \tag{9}$$

$$\dot{\mathbf{x}}_\mathbf{c} = \mathbf{F x_c} - \mathbf{G C_{trck} C x} + \mathbf{G y_{cmd}}. \tag{10}$$

In augmented matrix form, the system can be written as:

$$\begin{bmatrix} \dot{\mathbf{x}} \\ \dot{\mathbf{x}}_\mathbf{c} \end{bmatrix} = \underbrace{\begin{bmatrix} \mathbf{A_{fw}} & \mathbf{B\Lambda H} \\ -\mathbf{G C_{trck} C} & \mathbf{F} \end{bmatrix}}_{\mathbf{A_a}} \underbrace{\begin{bmatrix} \mathbf{x} \\ \mathbf{x_c} \end{bmatrix}}_{\mathbf{x_a}} - \underbrace{\begin{bmatrix} \mathbf{B} \\ \mathbf{0}_{n_c \times m} \end{bmatrix}}_{\mathbf{B_a}} \mathbf{\Lambda K^T C_{sas}} \underbrace{\begin{bmatrix} \mathbf{C} & \mathbf{0}_{p \times n_c} \end{bmatrix}}_{\mathbf{C_a}} \begin{bmatrix} \mathbf{x} \\ \mathbf{x_c} \end{bmatrix} + \underbrace{\begin{bmatrix} \mathbf{B\Lambda J} \\ \mathbf{G} \end{bmatrix}}_{\mathbf{B_{ref}}} \mathbf{y_{cmd}}, \tag{11}$$

or in shorter form:

$$\dot{\mathbf{x}}_\mathbf{a} = \mathbf{A_a x_a} - \mathbf{B_a \Lambda K^T C_{sas} C_a x_a} + \mathbf{B_{ref} y_{cmd}}, \tag{12}$$

$$\mathbf{y} = \mathbf{C_a x_a}. \tag{13}$$

Considering the ideal solution as the reference model, i.e., doing $\mathbf{x_a} = \mathbf{x_{ref}}$ and $\mathbf{y} = \mathbf{y_{ref}}$:

$$\dot{\mathbf{x}}_\mathbf{ref} = \underbrace{\left(\mathbf{A_a} - \mathbf{B_a \Lambda K^T C_{sas} C_a}\right)}_{\mathbf{A_{ref}}} \mathbf{x_{ref}} + \mathbf{B_{ref} y_{cmd}} = \mathbf{A_{ref} x_{ref}} + \mathbf{B_{ref} y_{cmd}}, \tag{14}$$

$$\mathbf{y_{ref}} = \mathbf{C_a x_{ref}}, \tag{15}$$

where $\mathbf{x_{ref}} \in \mathbb{R}^{(n+n_c)\times 1}$ and $\mathbf{y_{ref}} \in \mathbb{R}^{p\times 1}$ are the reference state and output vectors, respectively. From Equations (7-9) it is straightforward that $\mathbf{e_y} \in \mathbb{R}^{p_{trck}\times 1}$, $\mathbf{u_c} \in \mathbb{R}^{m\times 1}$, $\mathbf{K^T} \in \mathbb{R}^{m\times p_{sas}}$, $\mathbf{C_{sas}} \in \mathbb{R}^{p_{sas}\times p}$, $\mathbf{C_{trck}} \in \mathbb{R}^{p_{trck}\times p}$ and $\mathbf{y_{cmd}} \in \mathbb{R}^{p_{trck}\times 1}$.

In Equation (14), the expression:

$$\mathbf{A_{ref}} = \left(\mathbf{A_a} - \mathbf{B_a \Lambda K^T C_{sas} C_a}\right) \tag{16}$$

is called matching condition, and the design of the adaptive law assumes the existence of a constant (possibly unknown) gain matrix $\mathbf{K^T}$ that must satisfy it. Or, in other words, given a reference Hurwitz matrix $\mathbf{A_{ref}}$, there exist an ideal $\mathbf{K^T}$ such that the matching condition must be satisfied.

The problem is that once the systems parameters $\mathbf{A}$ and $\mathbf{\Lambda}$ are unknown, nor the ideal gain matrix $\mathbf{K^T}$ and, consequently, neither $\mathbf{u_{sas}}$ can be computed directly. Instead, the adaptive control law given by Equation (3) is considered. Then, the augmented dynamics of the real closed-loop system is given in terms of an adaptive (or estimated) gain matrix $\hat{\mathbf{K}}^\mathbf{T} \in \mathbb{R}^{m\times p_{sas}}$, whose dynamics will be defined later through the inverse Lyapunov analysis:

$$\dot{\mathbf{x}}_\mathbf{a} = \mathbf{A_a x_a} - \mathbf{B_a \Lambda \hat{K}^T C_{sas} C_a x_a} + \mathbf{B_{ref} y_{cmd}}. \tag{17}$$

The interest here is to design an adaptive control law such that the augmented system state $\mathbf{x_a}$ globally uniformly and asymptotically tracks the state of the reference model $\mathbf{x_{ref}}$. It is also

required that during tracking, all the other signals in the closed-loop remain uniformly bounded. Thus, for any bounded command $\mathbf{y_{cmd}}$, the control input $\hat{\mathbf{u}}_{\mathbf{sas}}$ must be chosen such that the state tracking error:

$$\mathbf{e} = \mathbf{x_a} - \mathbf{x_{ref}} \tag{18}$$

globally uniformly and asymptotically tends to zero, i.e.:

$$\lim_{t\to\infty} \|\mathbf{x_a(t)} - \mathbf{x_{ref}(t)}\| = \mathbf{0}. \tag{19}$$

Subtracting Equation (14) from Equation (17), and using the relation given in Equation (16) it is possible to compute the closed-loop dynamic of the state tracking error vector:

$$\begin{aligned}
\dot{\mathbf{x}}_\mathbf{a} - \dot{\mathbf{x}}_\mathbf{ref} &= \mathbf{A_a x_a} - \mathbf{B_a \Lambda \hat{K}^T C_{sas} C_a x_a} + \mathbf{B_{ref} y_{cmd}} - \mathbf{A_{ref} x_{ref}} - \mathbf{B_{ref} y_{cmd}} \Leftrightarrow \\
\dot{\mathbf{e}} &= \left(\mathbf{A_{ref}} + \mathbf{B_a \Lambda K^T C_{sas} C_a}\right)\mathbf{x_a} - \mathbf{B_a \Lambda \hat{K}^T C_{sas} C_a x_a} + \mathbf{B_{ref} y_{cmd}} \\
&\quad -\mathbf{A_{ref} x_{ref}} - \mathbf{B_{ref} y_{cmd}} \\
&= \mathbf{A_{ref}}\left(\mathbf{x_a} - \mathbf{x_{ref}}\right) + \mathbf{B_a \Lambda}\left(\mathbf{K} - \hat{\mathbf{K}}\right)^T \mathbf{C_{sas} C_a x_a} \\
&= \mathbf{A_{ref} e} + \mathbf{B_a \Lambda \Delta K}^T \mathbf{C_{sas} C_a x_a},
\end{aligned} \tag{20}$$

where $\mathbf{\Delta K} = \mathbf{K} - \hat{\mathbf{K}}$ represents the gain estimation error.

A Lyapunov-based approach [9] can now be applied, eventually leading to the design of stable adaptive laws and a satisfactory closed-loop system tracking performance. The main idea is choose a Lyapunov function candidate and then select an adaptive law such that the function time derivative becomes nonpositive, when evaluated along the trajectories of the error dynamic (Equation (20)). Consider a radially unbounded quadratic Lyapunov function candidate in the form:

$$V\left(\mathbf{e}, \mathbf{\Delta K}\right) = \mathbf{e^T P_{ref} e} + trace\left(\mathbf{\Delta K^T \Gamma_x^{-1} \Delta K \Lambda}\right), \tag{21}$$

where $\mathbf{\Gamma_x} = \mathbf{\Gamma_x^T} > \mathbf{0}$ is a rate of adaptation and $\mathbf{P_{ref}} = \mathbf{P_{ref}^T} > \mathbf{0}$ is the unique symmetric positive-definite solution of the algebraic Lyapunov equation:

$$\mathbf{P_{ref} A_{ref}} + \mathbf{A_{ref}^T P_{ref}} = -\mathbf{Q}, \tag{22}$$

with some $\mathbf{Q} = \mathbf{Q^T} > \mathbf{0}$.The time derivative of V is:

$$\dot{V}\left(\mathbf{e}, \mathbf{\Delta K}\right) = \dot{\mathbf{e}}^\mathbf{T} \mathbf{P_{ref} e} + \mathbf{e^T P_{ref}} \dot{\mathbf{e}} + \frac{d}{dt}\left[trace\left(\mathbf{\Delta K^T \Gamma_x^{-1} \Delta K \Lambda}\right)\right]. \tag{23}$$

Now, substituting Equation (20) into Equation (23) we have:

$$\begin{aligned}
\dot{V}\left(\mathbf{e}, \mathbf{\Delta K}\right) &= \left(\mathbf{A_{ref} e} + \mathbf{B_a \Lambda \Delta K}^T \mathbf{C_{sas} C_a x_a}\right)^T \mathbf{P_{ref} e} \\
&\quad + \mathbf{e^T P_{ref}}\left(\mathbf{A_{ref} e} + \mathbf{B_a \Lambda \Delta K}^T \mathbf{C_{sas} C_a x_a}\right) - 2trace\left(\mathbf{\Delta K^T \Gamma_x^{-1} \dot{\hat{K}} \Lambda}\right) \\
&= \mathbf{e}^T \mathbf{A_{ref}}^T \mathbf{P_{ref} e} + \left(\mathbf{B_a \Lambda \Delta K}^T \mathbf{C_{sas} C_a x_a}\right)^T \mathbf{P_{ref} e} + \mathbf{e^T P_{ref} A_{ref} e} \\
&\quad + \mathbf{e^T P_{ref}}\left(\mathbf{B_a \Lambda \Delta K}^T \mathbf{C_{sas} C_a x_a}\right) - 2trace\left(\mathbf{\Delta K^T \Gamma_x^{-1} \dot{\hat{K}} \Lambda}\right) \\
&= \mathbf{e^T}\left(\mathbf{A_{ref}}^T \mathbf{P_{ref}} + \mathbf{P_{ref} A_{ref}}\right)\mathbf{e} + 2\mathbf{e^T P_{ref}}\left(\mathbf{B_a \Lambda \Delta K}^T \mathbf{C_{sas} C_a x_a}\right) \\
&\quad - 2trace\left(\mathbf{\Delta K^T \Gamma_x^{-1} \dot{\hat{K}} \Lambda}\right),
\end{aligned} \tag{24}$$

and using Equation (22):

$$\dot{V}\big(\mathbf{e}, \mathbf{\Delta K}\big) = -\mathbf{e^T Q e} + 2\mathbf{e^T P_{ref}}\big(\mathbf{B_a \Lambda \Delta K}^T \mathbf{C_{sas} C_a x_a}\big) - 2trace\big(\mathbf{\Delta K^T \Gamma_x^{-1} \dot{\hat{K}} \Lambda}\big). \quad (25)$$

Via the vector trace indentity $\mathbf{a}^T\mathbf{b} = trace\big(\mathbf{b a}^T\big)$:

$$\underbrace{\mathbf{e^T P_{ref} B_a \Lambda}}_{\mathbf{a}^T} \underbrace{\mathbf{\Delta K}^T \mathbf{C_{sas} C_a x_a}}_{\mathbf{b}} = trace\left(\underbrace{\mathbf{\Delta K}^T \mathbf{C_{sas} C_a x_a}}_{\mathbf{b}} \underbrace{\mathbf{e^T P_{ref} B_a \Lambda}}_{\mathbf{a}^T} \right). \quad (26)$$

Substituting Equation (26) into Equation (25):

$$\begin{aligned} \dot{V}\big(\mathbf{e}, \mathbf{\Delta K}\big) &= -\mathbf{e^T Q e} + 2trace\Big(-\mathbf{\Delta K^T \Gamma_x^{-1} \dot{\hat{K}} \Lambda} + \mathbf{\Delta K}^T \mathbf{C_{sas} C_a x_a e^T P_{ref} B_a \Lambda} \Big) \\ &= -\mathbf{e^T Q e} + 2trace\Big(\mathbf{\Delta K^T} \Big[-\mathbf{\Gamma_x^{-1} \dot{\hat{K}}} + \mathbf{C_{sas} C_a x_a e^T P_{ref} B_a} \Big] \mathbf{\Lambda} \Big). \end{aligned} \quad (27)$$

If the adaptive law is selected as:

$$\begin{aligned} \mathbf{\dot{\hat{K}}} &= \mathbf{\Gamma_x C_{sas} C_a x_a e^T P_{ref} B_a} \\ &= \mathbf{\Gamma_x y_{sas} e^T P_{ref} B_a}, \end{aligned} \quad (28)$$

then the time derivative of V in Equation (27) becomes globally negative semidefinite:

$$\dot{V}\big(\mathbf{e}, \mathbf{\Delta K}\big) = -\mathbf{e^T Q e} \leq 0. \quad (29)$$

Therefore, the closed-loop error dynamic is uniformly stable. So, the state tracking error $\mathbf{e}$ and parameter estimation error $\mathbf{\Delta K}$ are uniformly bounded and so is the adaptive gain $\mathbf{\hat{K}}$. Since $\mathbf{y_{cmd}}$ is bounded, and $\mathbf{A_{ref}}$ is Hurwitz, then $\mathbf{x_{ref}}$ and $\mathbf{\dot{x}_{ref}}$ are bounded (Equation (14)). Once $\mathbf{e}$ and $\mathbf{x_{ref}}$ are bounded, it is straightforward that $\mathbf{x_a}$ is uniformly bounded, and consequently $\mathbf{\hat{u}_{sas}}$ in Equation (3) as well as $\mathbf{y}$ in Equation (13) will also be. This, in turn, ensures that $\mathbf{u_c}$ is bounded and so $\mathbf{u}$ as well. The latter implies that $\mathbf{\dot{x}_a}$ is bounded, and thus, $\mathbf{\dot{e}}$ is bounded. Furthermore, the second time derivative of V:

$$\ddot{V} = -2\mathbf{e^T Q \dot{e}} \quad (30)$$

is bounded, once $\mathbf{e}$ and $\mathbf{\dot{e}}$ are bounded, and so $\dot{V}$ is uniformly continuous. Since in addition V is lower bounded and $\dot{V} \leq 0$, then using Barbalat's lemma it is possible to demonstrate:

$$\lim_{t\to\infty} \dot{V}(t) = 0, \quad (31)$$

which implies:

$$\lim_{t\to\infty} \mathbf{e}(t) = \mathbf{0}. \quad (32)$$

This is the formal proof that the state tracking error tends to the origin globally, uniformly and asymptotically. As a result, Equation (19) is satisfied and the real plant tracks the reference model. Table 1 summarizes the MIMO MRAC design equations proposed in this work.

Augmented open-loop plant	$\dot{\mathbf{x}}_\mathbf{a} = \begin{bmatrix} \mathbf{A} & \mathbf{0} \\ -\mathbf{G}\mathbf{C}_\mathbf{trck}\mathbf{C} & \mathbf{F} \end{bmatrix} \mathbf{x}_\mathbf{a} + \begin{bmatrix} \mathbf{B}\boldsymbol{\Lambda} \\ \mathbf{0} \end{bmatrix} \mathbf{u} + \begin{bmatrix} \mathbf{0} \\ \mathbf{G} \end{bmatrix} \mathbf{y}_\mathbf{cmd}$
Reference model	$\dot{\mathbf{x}}_\mathbf{ref} = \mathbf{A}_\mathbf{ref}\mathbf{x}_\mathbf{ref} + \mathbf{B}_\mathbf{ref}\mathbf{y}_\mathbf{cmd}$
Model matching conditions	$\mathbf{A}_\mathbf{ref} = \left(\mathbf{A}_\mathbf{a} - \mathbf{B}_\mathbf{a}\boldsymbol{\Lambda}\mathbf{K}^\mathbf{T}\mathbf{C}_\mathbf{sas}\mathbf{C}_\mathbf{a}\right)$
State tracking error	$\mathbf{e} = \mathbf{x}_\mathbf{a} - \mathbf{x}_\mathbf{ref}$
SAS control input	$\hat{\mathbf{u}}_\mathbf{sas} = \hat{\mathbf{K}}^\mathbf{T}\mathbf{C}_\mathbf{sas}\mathbf{C}\mathbf{x}$
Algebraic Lyapunov equation	$\mathbf{P}_\mathbf{ref}\mathbf{A}_\mathbf{ref} + \mathbf{A}_\mathbf{ref}^\mathbf{T}\mathbf{P}_\mathbf{ref} = -\mathbf{Q}$
MIMO MRAC law	$\dot{\hat{\mathbf{K}}} = \boldsymbol{\Gamma}_x\mathbf{y}_\mathbf{sas}\mathbf{e}^\mathbf{T}\mathbf{P}_\mathbf{ref}\mathbf{B}_\mathbf{a}$

Table 1: MIMO MRAC design equations

3 NUMERICAL APPLICATION

A case-study considering the flexible aircraft X-HALE will be adressed. Specifically, an adaptive SAS will be implemented to deal with the instability which arises applying linear control for velocity, altitude, sideslip and roll angle tracking, for a wide range of flight speeds, as described in the section 2.1.

3.1 Model description

The X-HALE is a flexible, high-aspect-ratio, wing-boom-tail type aircraft [1]. It has a 6 m-span wing, built up with six one-meter-span panels, and a chord of 0.2 m. The two outer panels of the wing have a dihedral angle of 10 degrees and each one has an aileron. The aircraft has five equidistant fuselages mounted under the wing to accommodate engines and instrumentation. It is composed of five horizontal stabilizers. The central one is only used in a flipping mode to increase the directional stability of the aircraft when in vertical tail configuration [4], thus reducing the pilot workload while operating the aircraft. The aircraft has an unstable mode[1] when the central stabilizer is in the horizontal position. The two outer horizontal stabilizers (elevons) of each side are used for active control and can be deflected in any possible combination. All elevons are conected to the wing with booms. The central and two inner booms have ventral fins for improvement of the lateral-directional stability. Figure 4 shows the aircraft's geometry without the ventral fins and the control inputs are indicated with the corresponding nomenclature.

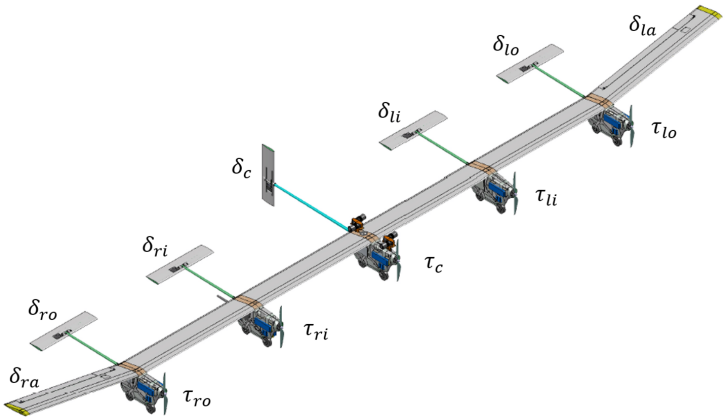

Figure 4: X-HALE geometry, control surfaces and engines.

[1] A combination of the Dutch-roll and wing bending modes.

X-HALE flight dynamics has been modelled according to general body axes formulation by Guimares Neto et al. [15], applicable to moderately flexible aircraft. Basically, the structural dynamics is characterized by a finite-element representation, assuming small elastic deformations and the incremental unsteady aerodynamics is modeled using the Doublet-Lattice Method [16] with rational function approoximations [17] and appropriate aerodynamic influence coefficient corrections to take viscous effects into account.

The model describes the dynamic equations of motion in the inertial reference frame, for all six degrees of freedom: displacements in the x and y directions, altitude H and roll, pitch and heading angles (ϕ, θ and ψ, respectively). Furthermore, the velocity V, the angle of attack α, the sideslip angle β, as well as the angular rates p, q and r are also described. A particular feature of the model is the modeling of the structural dynamics using modal amplitudes and their time-derivatives ($\boldsymbol{\eta}$ and $\dot{\boldsymbol{\eta}}$). Aerodynamic lag states arise due to global ("rigid-body") and control surfaces dynamics ($\boldsymbol{\lambda}_{\mathbf{rb}}$) and to the aeroelastic dynamics ($\boldsymbol{\lambda}_{\boldsymbol{\eta}}$). The state vector $\mathbf{x}$ is:

$$\mathbf{x} = \left[V,\, \alpha,\, q,\, \theta,\, H,\, x,\, \beta,\, \phi,\, p,\, r,\, \psi,\, y,\, \lambda^T_{rb_{84\times1}},\, \eta^T_{14\times1},\, \dot{\eta}^T_{14\times1},\, \lambda^T_{\eta_{98\times1}}\right]^T \tag{33}$$

Seven control sufaces, including four elevons (δ_{ro}, δ_{ri}, δ_{li}, δ_{lo}), one central stabilizer (δ_c) and two ailerons (δ_{ra}, δ_{la}), and five engines (τ_{ro}, τ_{ri}, τ_c, τ_{li}, τ_{lo}) give the control input of the X-HALE, as seen in Figure 4. The system contain a total of 12 inputs:

$$\mathbf{u} = \left[\delta_{la},\, \delta_{lo},\, \delta_{li},\, \delta_c,\, \delta_{ri},\, \delta_{ro},\, \delta_{ra},\, \tau_{lo},\, \tau_{li},\, \tau_c,\, \tau_{ri},\, \tau_{ro}\,\right]^T \tag{34}$$

where ($\dot{\bullet}$) is the time derivative, the subscript l means left side of the aircraft, r right side, o outer, i inner and c central position. In this application pitch attitude will be controlled by the inner elevons (δ_{li} and δ_{ri}), operating symmetrically, while roll angle will be controlled by the outer elevons (δ_{lo} and δ_{ro}), operating antisymmetrically. Yawing motion will be controlled using differential thrust from the engines. Ailerons will be employed for shape control. Thus, the input matrix becomes:

$$\mathbf{B_{mix}} = \mathbf{B}\big(\,:, [(3+5)\ (15+16+17+18+19)\ (15+16-18-19)\ (2-6)\ 1\ 7]\,\big) \tag{35}$$

where $\mathbf{B_{mix}} \in \mathbb{R}^{222\times6}$ and the input vector is assumed to be:

$$\mathbf{u} = \left[\delta_e,\, \Pi,\, \delta_r,\, \delta_a,\, \delta_{la},\, \delta_{ra}\right]^T \tag{36}$$

where Π is a factor that expresses the relation between the total thrust of the aircraft and the trimmed one.

The 116 outputs comprises measurements such as displacements and attitude, linear and angular velocities, load factors, at different points of wings, stabilizers and pods. In addition, it is also possible to recover structural displacements and twists.

3.2 Baseline controller

The first step in the adaptive controller design is to determine a baseline linear controller which will be used in the reference model. This controller dictates the desirable closed-loop time-response characteristics. Assuming the architecture presented in Fig. 2, setting $\boldsymbol{\Lambda} = \mathbf{I_m}$ in

Equation (5) and assuming that $\mathbf{A}$ is known, the ideal SAS gain matrix $\mathbf{K^T}$ of the inner-loop has been calculated minimizing the linear quadratic cost index:

$$J = \frac{1}{2}\int_0^\infty \left(\mathbf{y_{sas}^T Q_{bl} y_{sas}} + \mathbf{u_{sas}^T R_{bl} u_{sas}}\right) dt \tag{37}$$

where $\mathbf{Q_{bl}}$ and $\mathbf{R_{bl}}$ are symmetric and positive definite weighting matrices. The outputs for the SAS ($\mathbf{y_{sas}}$) are θ, q, used as feedback signals to the elevator δ_e; ϕ, p, r, used as feedback signals to the outer elevons mixed in the lateral control command δ_a; and the structural displacements measured at the wing tips (T_z), fed back to left and right ailerons, δ_{la} and δ_{ra}. The choice of the cost index given in the Equation (37) ensures optimal regulation of the output $\mathbf{y_{sas}}$ around its trimmed condition with minimal control effort $\mathbf{u_{sas}}$.

For the outer loop, a controller was developed for velocity, altitude, sideslip and roll angle tracking. The outer loop controller has the structure presented in the Equation (7-8). The optimal design of matrices $\mathbf{F}$, $\mathbf{G}$, $\mathbf{H}$ and $\mathbf{J}$ was achieved by structured H_∞ synthesis using the *systune* MATLAB tool. The detailed development of this baseline controller is presented by Gonzales et. al [13, 18].

3.3 Simulation results

With the appropriated choice of the reference model, the next step is to design the MRAC system in order to recover the desired closed-loop performance, without any information about the parametric uncertainties. The design focus was on reducing undesired transient oscillations while providing adequate tracking response. After several iterations, the design parameters selected were:

$$\mathbf{Q} = \begin{bmatrix} 1e^{-2}\mathbf{I_9} & * & * & * & * \\ * & 1e^{-5}\mathbf{I_{84}} & * & * & * \\ * & * & 1e^{-2}\mathbf{I_{28}} & * & * \\ * & * & * & 1e^{-5}\mathbf{I_{98}} & * \\ * & * & * & * & 1e^{-2}\mathbf{I_8} \end{bmatrix}; \qquad \mathbf{\Gamma_x} = \mathbf{I_{p_{sas}}} \tag{38}$$

where $\mathbf{I_N}$ corresponds to the N-by-N identity matrix and $*$ are the appropriate zero matrices. In the $\mathbf{Q}$ matrix, the first row weights the rigid body states, while the second one weights the rigid body aerodynamic lag states, the third weights the elastic states, the fourth the elastic aerodynamic lag states and the fifth row weights the compesator states. It is worth mentioning that the variables x, y and ψ were ignored in the design, since there is no dependency of the other states on these three variables. Now, the adaptive law described in Tab. 1 is able to be implemented and simulated.

The performance of the proposed control scheme has been evaluated considering a simulation of an accelerated, coordinated turn manoeuvre, with smooth increment of 4 m/s in the final flight speed and 20 degrees for the bank angle. Altitude increment and sideslip angle were hold constant and equal to zero. Figures 5 to 9 present the time responses of the closed-loop nonlinear simulations. In the figures, the results corresponding to the application of linear control (considering the plant at 14 m/s) are also displayed for the matter of comparison, and are called "non-adaptive". The results assigned by "reference" correspond to the closed-loop linear model used as the reference model in the adaptive law.

Clearly the MRAC system is able to recover the closed-loop dynamics of the reference model. According to the Fig. 5, the commanded velocity is reached with an overshoot less than 1% and

null steady-state error. A similar result is observed for the bank angle tracking. On the other hand, the altitude presents small oscillations around the trim point and a steady-state error of 0.02% relative to the commanded altitude, and 0.05% relative to the reference model altitude. The first one is a direct result of no zero poles in the plant, i.e. no pure integrator. The latter probably occurs because of a slight difference between the DC gains presented by the real plant and the reference model, since the reference model was obtained for a lower velocity. Finally, the sideslip angle presents a variation of 2.5 degrees in relation to the commanded one and a very small steady state-error of 0.07 degree.

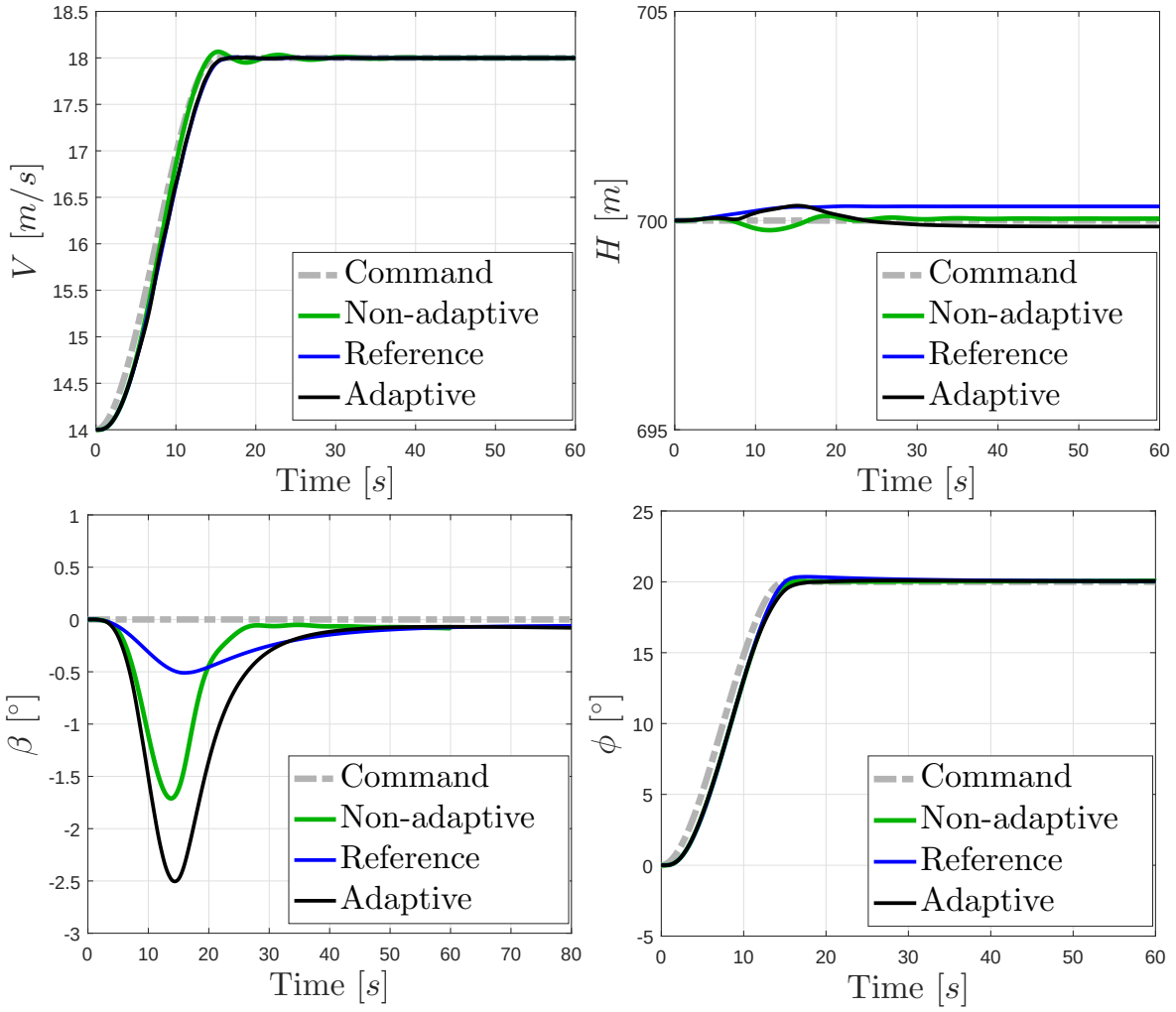

Figure 5: Closed-loop system tracking performance.

Roll rate response is shown in the left plot on Fig. 6. One can clearly see that after about 40s, an instability shows up in the response considering linear control (non-adaptive). In the right plot on the same figure, vertical displacements of left and right wings can be seen, and the same instability can be observed with non-adaptive control. The corresponding root-loci for increasing velocity can be seen in Fig. 7, where a pole corresponding to one of the aircraft elastic modes crosses the imaginary axis and gets unstable at 18 m/s. The corresponding modal shape, a third torsional mode, is shown on the same figure. Still in Fig. 6, the adaptive control law was able to avoid the referred instability, as the responses of roll rate p and wing tips displacements T_z attested. Additionally, for the adaptive case, the wing tip displacements stabilize in a condition where the deformations are larger, i.e. the wing bending increased. This is expected since

with the increase in velocity, and the resulting load factor of the turning maneuver, the aircraft stabilizes in a higher loading condition.

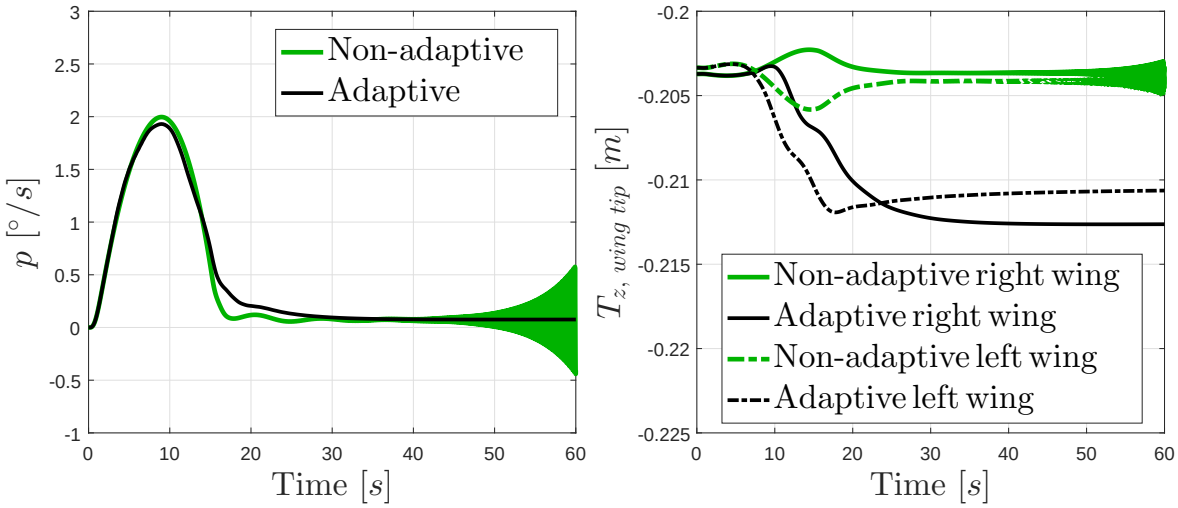

Figure 6: Nonadaptive system versus MRAC system.

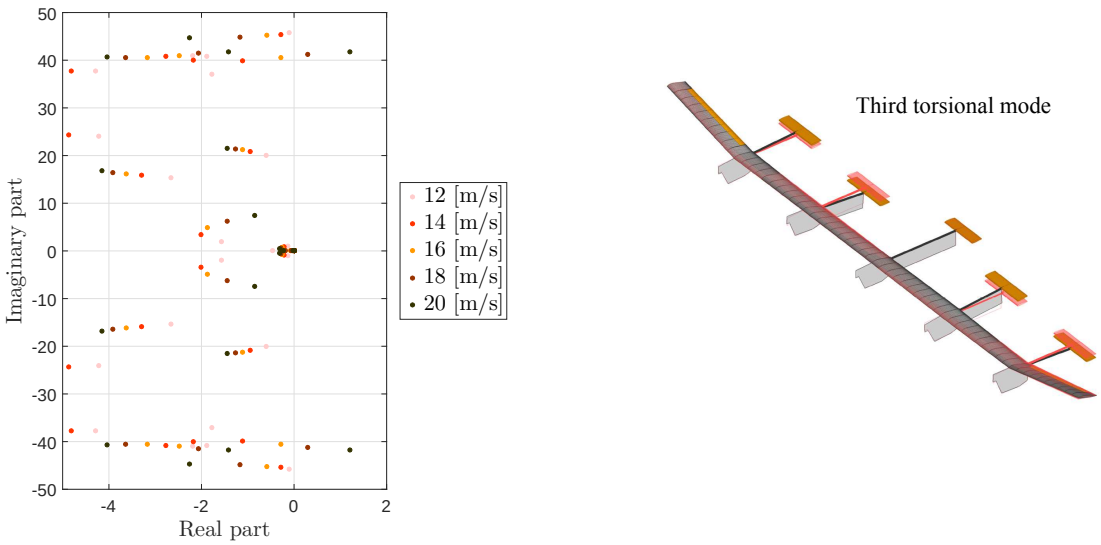

Figure 7: Root-loci of the closed-loop system considering linear (non-adaptive) control for increasing velocity.

Looking now to the control signals (Fig. 8), it is observed that all of them are feasible, that is, they operate with magnitudes smaller than the limits stipulated (± 25 degrees for the control surfaces and a thrust factor between 0 and 6), and the rate limits are not violated. To track the commanded velocity holding the trimmed altitude, all the engines accelerate in the first few seconds. The increase in velocity results in increased lift and, in turn, the aircraft tends to raise up its altitude. To compensate this effect, the inner elevons are deflected positively to regulate again the altitude of the aircraft to 700 m.

In the bank angle tracking, command reversal can be observed. It occurs due to the fact that the elevons are located at the ends of the booms, and their deflection cause a pitching moment that, as a result of the wing flexibility, changes the local angle of attack, leading to the opposite rolling behavior. Command reversal also has a direct effect on the ailerons used for shape control. The increase in the local angle of attack of the left half-wing generates a bending

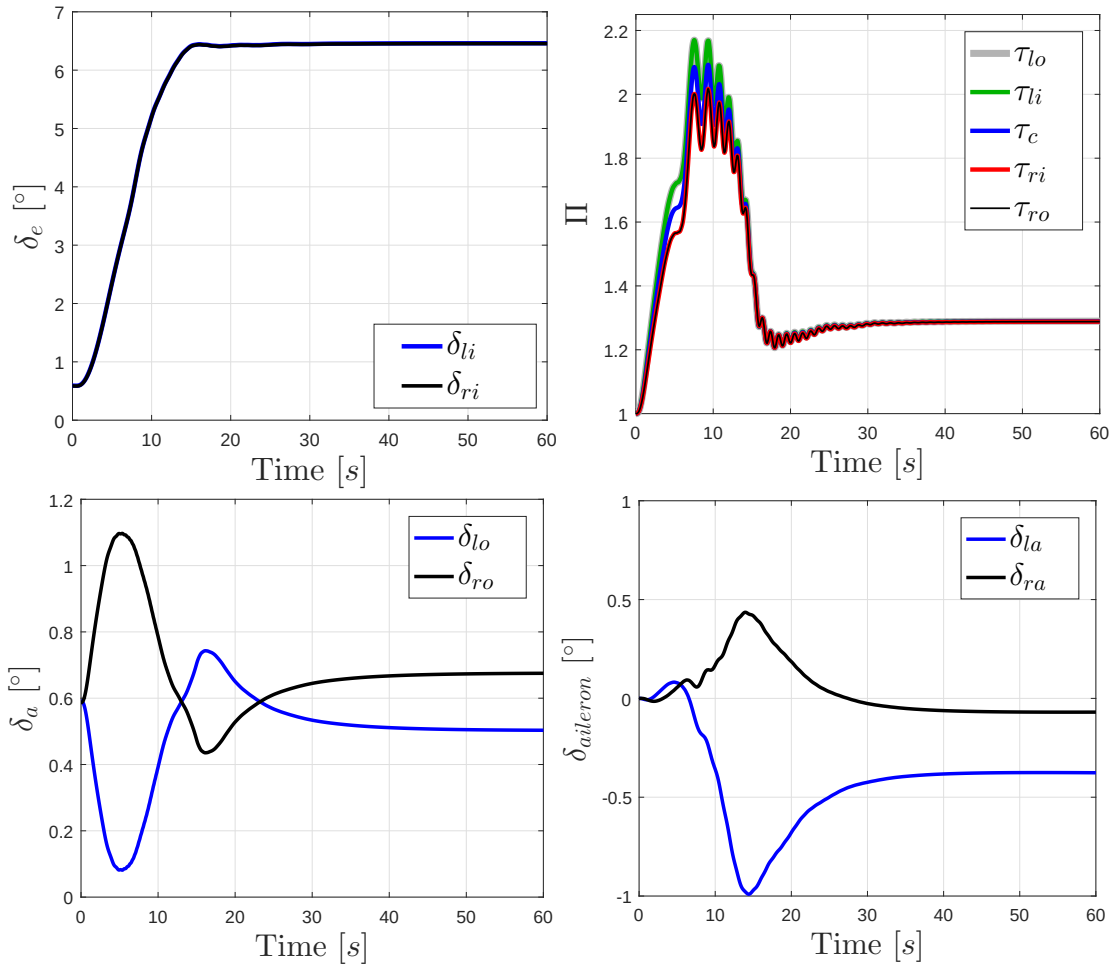

Figure 8: Input control signals.

moment at the wing root that deforms the left half-wing upwards, and the opposite occurs with the right half-wing. As a consequence, the left aileron deflects upwards (negative deflection) to control the shape, and similarly, the right aileron deflects downwards (positive deflection).

Finally, Fig. 9 presents the temporal evolution of the adaptive gains. The label $\hat{K}(i,:)$ in each plot means that the corresponding figure contains all gains of the i-th row of the adaptive gain matrix $\hat{\mathbf{K}}^{\mathbf{T}}$. In the legend, $\hat{K}(i,j)$ means that the corresponding line represents the time evolution of the adaptive gain located in the i-th row and j-th column. The gains were initialized in the simulation with their respective nominal values. It can be seen that gains with initial values different from zero varied very little in relation to their nominal value. On the other hand, some of the gains initialized to zero presented a more significant variation. The online adaptation of the gains ensures that the real closed-loop system behaves with desired stability and performance characteristics.

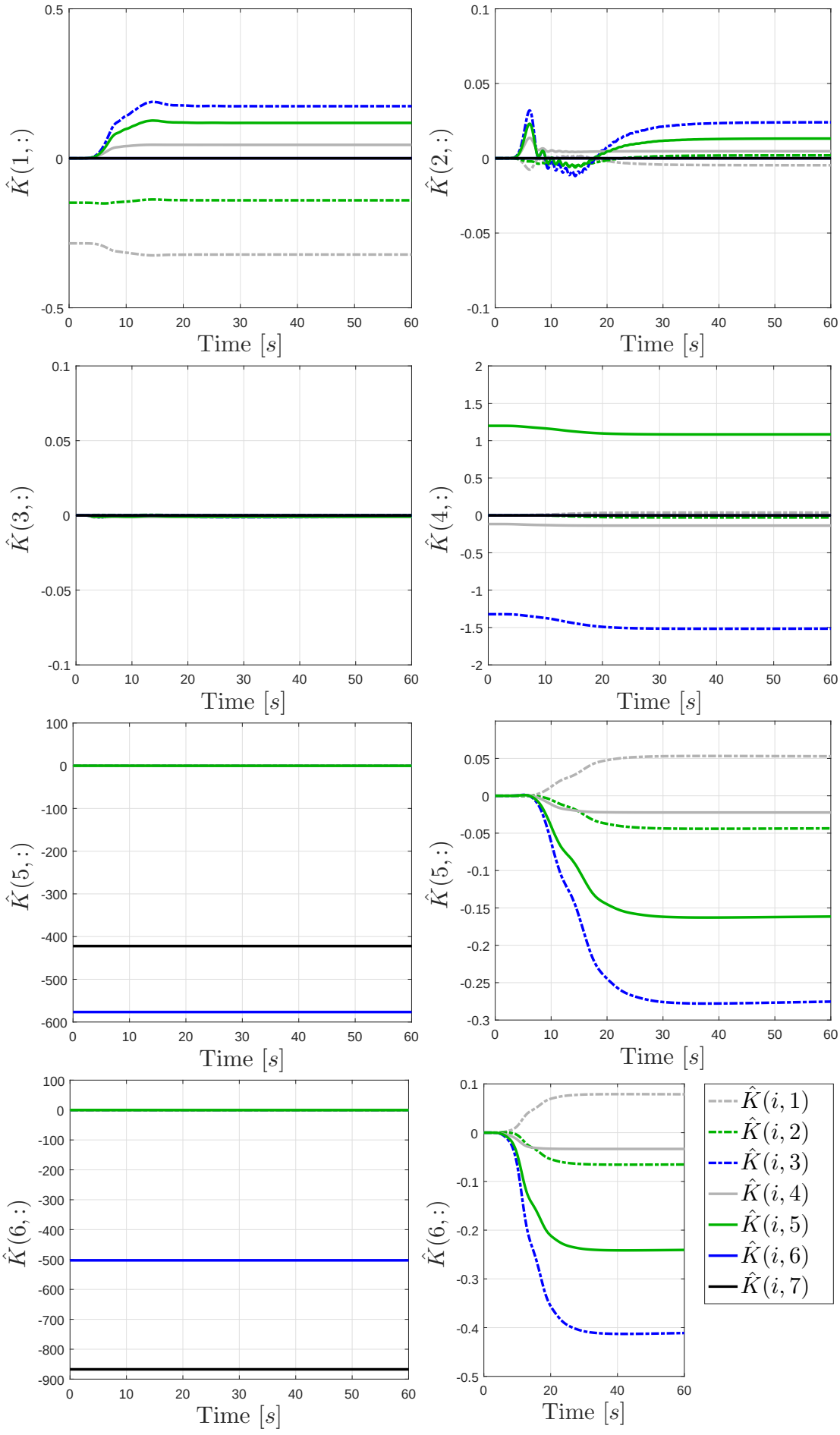

Figure 9: Evolution of adaptive gains.

4 CONCLUSION

In this work the design of a dynamic gain scheduling making use of an adaptive control law was addressed and applied to the trajectory control of a very flexible aircraft. It has been shown that for a classical tracking problem in which an aircraft is subject to large variations relative to the trimmed condition, linear control failed to hold stability. To overcome this problem, an online estimation of SAS gains was proposed. This estimation is done through an adaptive control law designed based on the dynamic behavior of a reference model.

An application for X-HALE aircraft has been implemented for the tracking of velocity, altitude, sideslip and roll angle. The nonlinear simulation results showed instabilities for large variations of commanded velocity when linear control was applied. On the other side, the proposed adaptive law was able to hold stability while ensuring the desired performance, without demanding excessive control effort.

A limitation of the control law proposed here is the assumption that all states of the system are measurable. In a future work, an alternative to deal with this problem will be addressed. Dicretization of the proposed adaptive controller will also be investigated for implementation on the real aircraft.

5 REFERENCES

[1] S. Cesnik, C. E., Senatore, P. J., Su, W., et al. (2012). X-hale: A very flexible unmanned aerial vehicle for nonlinear aeroelastic tests. *AIAA journal*, 50(12), 2820–2833.

[2] Jones, J. R. and Cesnik, C. E. S. (2013). Preliminary flight test correlations of the x-hale aeroelastic experiment. *International Forum on Aeroelasticity and Structural Dynamics*, 13.

[3] Newsroom, F. (2016). Aquilas first flight: A big milestone toward connecting billions of people.

[4] Cesnik, C. E. and Su, W. (2011). Nonlinear aeroelastic simulation of x-hale: a very flexible uav. In *49th AIAA Aerospace Sciences Meeting including the New Horizons Forum and Aerospace Exposition, Orlando, Florida*.

[5] Shearer, C. M. and Cesnik, C. E. (2007). Nonlinear flight dynamics of very flexible aircraft. *Journal of Aircraft*, 44(5), 1528–1545.

[6] Gibson, T. E., Annaswamy, A. M., and Lavretsky, E. (2011). Modeling for control of very flexible aircraft. In *Proceedings of the AIAA Guidance, Navigation, and Control Conference*.

[7] Cesnik, C. E. and Su, W. (2005). Nonlinear aeroelastic modeling and analysis of fully flexible aircraft. In *Proceedings of the 46th AIAA/ASME/ASCE/AHS/ASC Structures, Structural Dynamics and Materials Conference, Austin, TX*. pp. 2005–2169.

[8] Cesnik, C. E. S., Senatore, P. J., Su, W., et al. (2010). X-hale: A very flexible uav for nonlinear aeroelastic tests. *51 st AIAA/ASME/ASCE/AHS/ASC Structures, Structural Dynamics, and Materials Conference*, 23.

[9] Lavretsky, E. and Wise, K. (2013). Robust and adaptive control: With aerospace applications, ser. *Advanced textbooks in control and signal processing. London and New York: Springer*.

[10] Dydek, Z. T., Annaswamy, A. M., and Lavretsky, E. (2010). Adaptive control and the nasa x-15-3 flight revisited. *IEEE Control Systems*, 30(3), 32–48.

[11] Ponnusamy, S. S. and Guibé, J. B. (2012). Adaptive output feedback control of aircraft flexible modes. In *Communications, Computing and Control Applications (CCCA), 2012 2nd International Conference on*. IEEE, pp. 1–6.

[12] Qu, Z., Lavretsky, E., and Annaswamy, A. M. (2013). An adaptive controller for very flexible aircraft. In *AIAA Guidance, Navigation, and Control (GNC) Conference*. p. 4854.

[13] Gonzalez, P. J., Guimarães Neto, A. B., Chaves Barbosa, G., et al. (2017). X-hale autopilot with stability augmentation and shape control based on loop separation. In *International Forum on Aeroelasticity and Structural Dynamics*, 77. p. 19.

[14] Stevens, B. L. and Lewis, F. L. (2003). *Aircraft Control and Simulation*. New Delhi: Wiley India, 2 nd ed. ISBN: 978-81-265-2567-6.

[15] Guimarães Neto, A. B., Silva, R. G., Paglione, P., et al. (2016). Formulation of the flight dynamics of flexible aircraft using general body axes. *AIAA Journal*, 3516–3534.

[16] Albano, E. and Rodden, W. P. (1969). A doublet-lattice method for calculating lift distributions on oscillating surfaces in subsonic flows. *AIAA journal*, 7(2), 279–285.

[17] Eversman, W. and Tewari, A. (1991). Consistent rational-function approximation for unsteady aerodynamics. *Journal of Aircraft*, 28(9), 545–552.

[18] Gonzalez, P. J., Silvestre, F. J., Paglione, P., et al. (2016). Linear control of highly flexible aircraft based on loop separation. In *AIAA Atmospheric Flight Mechanics Conference,*. pp. 10.2514/6.2016–3398.

COPYRIGHT STATEMENT